Current-Gated Orthogonal Superconducting Transistor

Ruo-Peng Yu, ¹ Jin-Xin Hu, ¹ and Zi-Ting Sun^{1,*}

¹Department of Physics, The Hong Kong University of Science and Technology, Clear Water Bay, Hong Kong, China (Dated: November 4, 2025)

Nonreciprocal charge transport in superconductors enables rectification but is usually limited to the longitudinal direction. In this work, we show that a direct current bias injected off principal axes in two-dimensional anisotropic superconductors converts anisotropy into transverse nonreciprocity, enabling supercurrent diode effect measurement. This is demonstrated within both a Ginzburg-Landau framework and self-consistent mean-field calculations. When the control bias exceeds its critical value, the transverse dissipationless currents can only flow unidirectionally. This mechanism motivates the design of a multi-terminal current-gated orthogonal superconducting transistor (CGOST) and yields simple, bias direction angle-dependent design rules for device optimization. As direct applications, we propose a tunable supercurrent range controller and a half-wave rectifier based on the CGOST. Our findings open new avenues for developing nonreciprocal superconducting electronic devices.

I. INTRODUCTION

The superconducting diode effect (SDE), which is characterized by asymmetric critical currents $(|j_{c+}| \neq |j_{c-}|)$ in opposite directions, has emerged as a central theme of nonreciprocal superconducting transport and device physics. This phenomenon can be realized in both bulk superconductors [1–14] and Josephson junctions [15–35]. Conventionally, SDE requires the simultaneous breaking of spatial inversion and time-reversal symmetry (TRS). TRS breaking is typically achieved through external magnetic fields or intrinsic magnetic exchange, while inversion symmetry breaking can occur in noncentrosymmetric crystal structures, at interfaces via displacement fields, or through asymmetric sample geometries [1–11, 14–27, 30–34].

While nonreciprocal transport in superconductors has enabled rectification applications [36–38], most existing implementations are inherently longitudinal and rely on two-terminal configurations, which constrain functional diversity and design flexibility. Furthermore, the requirement for explicit symmetry breaking increases device complexity and introduces challenges in control, tunability, and integration.

In this work, we propose a new scheme overcoming these two limitations simultaneously: converting the crystalline or pairing anisotropy of a superconductor into transverse nonreciprocity through a multiterminal current-gated orthogonal superconducting transistor (CGOST). The device architecture is illustrated in Fig. 1(a), consisting of a two-dimensional (2D) anisotropic superconductor with a two-fold symmetry patterned into a disk-like geometry with multiple terminals. A direct current (DC) bias j_{bias} is injected along a direction θ deliberately misaligned with the material's principal axes (dashed lines) through a control terminal. Critically, the transverse critical currents $j_{mc\pm}$, measured

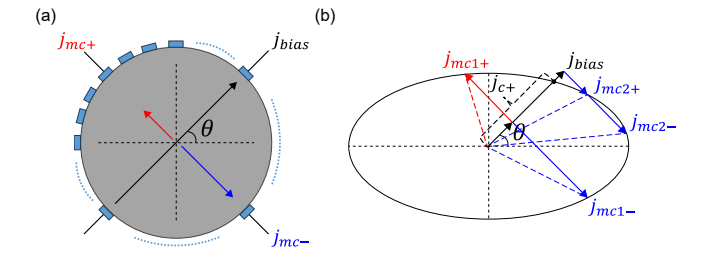


Fig. 1. (a) Schematic of CGOST, the bias current j_{bias} is applied along the direction of the black arrow (control terminal), and we measure the transverse critical currents $j_{mc\pm}$ (function terminal) in the direction vertical to the bias. (b) The working mechanism of CGOST is based on a two-fold anisotropic superconductor. The distribution of critical current shows an elliptical pattern. The critical currents with positive (j_{mc1+}) and negative $(j_{mc2+}, j_{mc1-} \text{ and } j_{mc2-})$ transverse components are labeled in red and blue, respectively. When j_{\parallel} is within the range of the ellipse, j_m can be either positive or negative $(j_{mc1-} \leq j_m \leq j_{mc1+})$, but when j_{\parallel} is greater than the critical current along the bias direction $j_{c+}(\theta)$, j_m can only be negative $(j_{mc2-} \leq j_m \leq j_{mc2+} < 0)$.

orthogonally to the bias direction through function terminals, will exhibit pronounced asymmetry (Fig. 1(b)), with neither TRS nor inversion symmetry breaking.

Using phenomenological Ginzburg-Landau (GL) theory and self-consistent mean-field (MF) calculations, we reveal that: depairing critical currents in anisotropic superconductors form an elliptical envelope [Fig. 1(b)]. The control bias selects a finite-momentum condensate and effectively shifts the reference point for transverse current measurements. This geometric effect immediately produces $|j_{mc+}| \neq |j_{mc-}|$ —a transverse SDE emerging purely from anisotropy conversion. Remarkably, when the bias exceeds the forward critical current along its own direction, $j_{\text{bias}} \geq j_{c+}(\theta)$, both transverse critical currents $j_{mc\pm}$ acquire the same sign. In this unidirectional regime, supercurrent can flow dissipationlessly only in one transverse direction while being completely

^{*} Contact author: zsunaw@connect.ust.hk

suppressed in the opposite direction—a phenomenon we identify as bias-induced unidirectional superconductivity (USC) [12]. This represents a qualitative advance beyond conventional diode behavior, enabling perfect on/off switching controlled entirely by current rather than external fields.

Additionally, we establish several key results: (i) Both normal-state anisotropy (anisotropic Fermi velocities in s-wave superconductors) and pairing-channel anisotropy (nematic p-wave pairing with isotropic Fermi surfaces) can be used to realize the CGOST, broadening the material platform; (ii) the proposal naturally extends to hightemperature superconductors (high- T_c SCs) with fourfold rotational symmetry, such as d-wave cuprates, significantly expanding operational temperature and current magnitude ranges; (iii) Device performance can be systematically optimized through simple angle-dependent design rules (by choosing the direction of bias); and (iv) two immediate applications are demonstrated: a tunable supercurrent range controller [39] and the half-wave rectifier [37, 38] with adjustable rectification windows. These findings establish CGOST as a versatile, multiterminal building block for current-controlled superconducting electronics.

II. GINZBURG-LANDAU THEORY OF ANISOTROPIC SUPERCONDUCTORS

Without loss of generality, we consider the GL theory of a 2D superconductor with two-fold rotational symmetry to begin with (the formalism for generic anisotropic superconductors can refer to **Appendix A**), which can arise from the nematicity in the normal state of a conventional superconductor as in Ising superconductors [40–44] like monolayer T_d -MoTe₂ [45, 46], and in kagome superconductors AV_3Sb_5 (A=K, Rb, Cs) [47–51], or from the anisotropic pairing such as nematic p-wave superconductors (see **Appendix C**) with two-fold rotational symmetry [52–54], even with isotropic Fermi velocities.

From a general perspective, we begin with the phenomenological GL free energy, which reads

$$F = \int d\mathbf{r} \{ \frac{1}{2m_x} |\partial_x \Psi|^2 + \frac{1}{2m_y} |\partial_y \Psi|^2 + \alpha |\Psi|^2 + \beta |\Psi|^4 \},$$
(1)

where m_x and m_y are effective mass along the x and y-directions and $m_x \neq m_y$ describes the anisotropy. α and β are GL coefficients. To describe the current-carrying superconducting state, we perform the Fourier transformation on the order parameter as $\Psi \equiv \Psi(\mathbf{r}) = \frac{1}{\sqrt{\Omega}} \sum_{\mathbf{q}} \Psi_{\mathbf{q}} e^{i\mathbf{q} \cdot \mathbf{r}}$, and restrict the analysis to a single- \mathbf{q} state selected by the injecting current. The free energy density for the center of mass momentum \mathbf{q} state reads

$$\mathcal{F}(\boldsymbol{q}) = \left(\frac{q_x^2}{2m_x} + \frac{q_y^2}{2m_y} + \alpha\right) |\Psi_{\boldsymbol{q}}|^2 + \beta |\Psi_{\boldsymbol{q}}|^4, \quad (2)$$

where $\beta > 0$ and $\mathbf{q} = (q_x, q_y)$ satisfies $q_x^2/m_x + q_y^2/m_y + 2\alpha < 0$ in the superconducting regime. Then the supercurrent density can be obtained as (Eq. (A2)):

$$\mathbf{j}(\mathbf{q}) = -\frac{e}{\beta} \left[\alpha + \frac{1}{2} \left(\frac{q_x^2}{m_x} + \frac{q_y^2}{m_y} \right) \right] \left(\frac{q_x}{m_x} \hat{x} + \frac{q_y}{m_y} \hat{y} \right).$$
(3)

To evaluate the depairing currents $j_{c\pm}(\theta)$ along an arbitrary direction $\hat{\theta} = (\cos \theta, \sin \theta)$ (for simplicity, we set $0 < \theta < \pi/2$), we solve the momenta $q_c(\theta)$ corresponding to the critical current, yielding

$$q_c(\theta) = \pm \frac{\sqrt{2|\alpha|} \left(m_x \cos \theta, m_y \sin \theta \right)}{\sqrt{3 \left(m_x \cos^2 \theta + m_y \sin^2 \theta \right)}}.$$
 (4)

Thus the domain \mathcal{D} of all physical current-carrying states \boldsymbol{q} is contained by the envelope of $\boldsymbol{q}_c(\theta)$: $q_x^2/m_x+q_y^2/m_y<2|\alpha|/3$, which is consistent with the previous constraint $q_x^2/m_x+q_y^2/m_y<2|\alpha|$ of \boldsymbol{q} . Substituting Eq. (4) into Eq. (3), we have

$$j_{c\pm}(\theta) = \pm \frac{e}{\beta} \sqrt{\frac{8|\alpha|^3}{27\left(m_x \cos^2 \theta + m_y \sin^2 \theta\right)}}.$$
 (5)

In this way, m_x/m_y can be obtained from the experimental measurement of the critical current by $m_x/m_y = (j_{c\pm}(\pi/2)/j_{c\pm}(0))^2$.

III. TRANSVERSE SUPERCONDUCTING DIODE EFFECT FROM DC BIAS

Following our proposal in Fig. 1 (b), now we apply a DC bias and measure the transverse critical current. Assuming that the bias current j_{bias} is applied along the $\hat{\theta}$ direction, then the radical component j_{\parallel} of the total current is (Eq. (A6)):

$$j_{\parallel} = -\frac{e}{\beta} \left[\alpha + \frac{1}{2} \left(\frac{q_x^2}{m_x} + \frac{q_y^2}{m_y} \right) \right] \left(\frac{q_x \cos \theta}{m_x} + \frac{q_y \sin \theta}{m_y} \right), \tag{6}$$

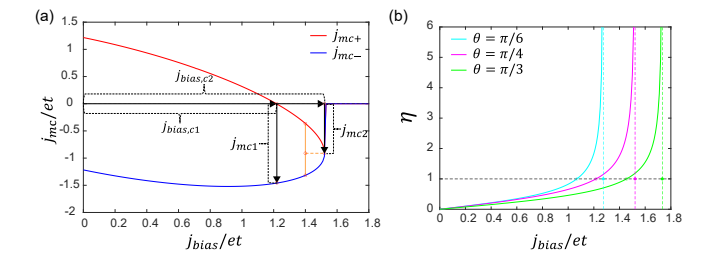


Fig. 2. (a) The evolution of j_{mc+} and j_{mc-} (labeled as red and blue lines respectively) with increasing j_{bias} , j_{mc+} becomes negative when $j_{bias} > j_{bias,c1} = 1.217et$. Here we set $\theta = \pi/4$. (b) The diode efficiency $\eta(j_{bias})$ for three different θ . Parameters used here: $\alpha = -0.5t, \beta = 0.1t, m_x = 4/t, m_y = 1/t$. t is an arbitrary unit.

where we fix $j_{\parallel} = j_{bias}$. The measured current in the transverse direction is (Eq. (A7)):

$$j_m = -\frac{e}{\beta} \left[\alpha + \frac{1}{2} \left(\frac{q_x^2}{m_x} + \frac{q_y^2}{m_y} \right) \right] \left(\frac{q_x \sin \theta}{m_x} - \frac{q_y \cos \theta}{m_y} \right). \tag{7}$$

In Fig. 2(a) we show how the measured critical currents $j_{mc\pm}$ evolve as j_{bias} increases. When $j_{bias}=0$ we have $|j_{mc+}|=|j_{mc-}|$, and when $j_{bias}\neq0$ we immediately have $|j_{mc+}|\neq|j_{mc-}|$, which means that SDE can be observed in the transverse direction when the bias current j_{bias} is applied. We can also see this from the diode efficiency, which is defined as

$$\eta = \left| \frac{j_{mc+} + j_{mc-}}{j_{mc+} - j_{mc-}} \right|. \tag{8}$$

As shown in Fig. 2(b), η increases monotonically with j_{bias} for different bias directions $\hat{\theta}$, and for small j_{bias} limit, η is linear in j_{bias} as (substituting Eq. (B2) from **Appendix B** into Eq. (8)):

$$\eta \approx \frac{\beta}{e} \left(\frac{3}{2|\alpha|} \right)^{3/2} \frac{|(m_y - m_x)\sin\theta\cos\theta|}{\sqrt{m_x\sin^2\theta + m_y\cos^2\theta}} j_{bias}. \tag{9}$$

We can see that $\eta \neq 0$ as long as $m_x \neq m_y$ and $\hat{\theta}$ is deviated from high symmetry axes, which makes $\sin \theta$ or $\cos \theta$ vanish. At this regime, we seek a large slope $g(\theta)$ of $\eta = g(\theta)j_{bias}$, which takes its maximal value at $\tan \theta = \sqrt[4]{\frac{m_y}{m_x}}$, and the value is:

$$\max(g(\theta)) = \frac{\beta}{e} \left(\frac{3}{2|\alpha|} \right)^{3/2} \left| \sqrt{m_y} - \sqrt{m_x} \right|. \tag{10}$$

We notice that this previously overlooked phenomenon can be taken as an analogue of the crystal Hall effect [55] in anisotropic superconductors, where an electric field can drive a transverse Hall current in anisotropic metals, even with both TRS and inversion symmetry.

IV. UNIDIRECTIONAL REGIME

Surprisingly, when j_{bias} is greater than a critical value (we denote as $j_{bias,c1}$, the activation current of USC), we have $j_{mc-} < j_{mc+} < 0$ (or $j_{mc+} > j_{mc-} > 0$), i.e., the USC emerges in the transverse direction as a fully equilibrium state, which is shown in Fig. 2(a). If we further increase the bias current until $j_{bias} = j_{bias,c2}$, we have $j_{mc+} = j_{mc-} = j_{mc2}$ and then the superconductivity will cease. These features can also be seen from the diode efficiency η in Fig. 2(b), $\eta > 1$ when $j_{bias} > j_{bias,c1}$ and finally gets divergent when $j_{bias} = j_{bias,c2}$. A detailed discussion of the conditions for the USC region can be found in **Supplementary Information (SI) I** [56], where we have shown $j_{bias,c1} = j_{c+}(\theta)$.

To acquire a large USC operating range with a small activation current in CGOST, we introduce the USC quality factor $Q_{USC} = 1 - j_{bias,c1}/j_{bias,c2}$ and expect a larger value of Q_{USC} . As derived in **SI II** [56], the cease bias current $j_{bias,c2}$ is given by:

$$j_{bias,c2} = \frac{e}{\beta} \left(\frac{2|\alpha|}{3}\right)^{3/2} \sqrt{\frac{\cos^2 \theta}{m_x} + \frac{\sin^2 \theta}{m_y}}.$$
 (11)

So the USC quality factor $Q_{USC}(\theta)$ is

$$1 - \sqrt{\frac{m_x m_y}{(m_x \cos^2 \theta + m_y \sin^2 \theta)(m_y \cos^2 \theta + m_x \sin^2 \theta)}}.$$
(12)

It worth mention that that the maximum of $Q_{USC}(\theta)$ always locate at $\theta = \pi/4$, which is independent of the effective mass m_x and m_y , and:

$$\max(Q_{USC}) = Q_{USC}(\frac{\pi}{4}) = 1 - \frac{2\sqrt{m_x m_y}}{m_x + m_y}.$$
 (13)

We note that $\max(Q_{USC})$ reveals a simple relationship to the degree of anisotropy of the superconductor. It is symmetric with respect to m_x and m_y , and vanishes at the isotropic limit $m_x = m_y$. When $m_x/m_y < 1$ or $m_x/m_y > 1$, $\max(Q_{USC})$ towards unity monotonously as $m_x/m_y \to 0$ and $m_x/m_y \to \infty$, respectively. These features guide the design of CGOST.

Besides, the USC region can be used to make a supercurrent range controller in the functional terminal of CGOST [39], in which the nonvanishing supercurrent is restricted in the narrow, adjustable region between $[j_{mc-}, j_{mc+}]$ excludes zero current (the range highlighted in orange in Fig. 2(a)). The supercurrent range can be tuned from $[j_{mc1}, 0]$ (Fig. 2(a)), to a single value at j_{mc2} , by increasing j_{bias} from $j_{bias,c1}$ to $j_{bias,c2}$. Roughly speaking, the supercurrent is contained in a narrow range with width $j_{mc+} - j_{mc-} < |j_{mc1}|$ and center j_{mc2} , where the former can be adjusted by varying j_{bias} , while the tunability of the latter one relies on

$$j_{mc2} = \frac{e}{\beta} \left(\frac{2|\alpha|}{3}\right)^{3/2} \frac{(m_y - m_x)\sin\theta\cos\theta}{\sqrt{(m_x\sin^2\theta + m_y\cos^2\theta) m_x m_y}}.$$
(14)

The anisotropy and bias direction play decisive roles.

V. SELF-CONSISTENT MEAN-FIELD THEORY

To further support the analysis based on our phenomenological theory, we perform numerical calculations using self-consistent MF theory for a toy model on a square lattice. The normal-state dispersion is given by $\xi_{\boldsymbol{k}} = -2t_x \cos(k_x) - 2t_y \cos(k_y) - \mu$, where t_x and t_y are the hopping amplitudes along the x and y directions, and we set the lattice constant a=1 for simplicity. We mainly consider two cases: (i) a spin-singlet s-wave superconductor with anisotropic hopping $(t_x \neq t_y)$, and

(ii) a nematic spin-triplet p-wave superconductor with isotropic hopping. The schematics for these two cases are shown in Fig. 3(a) and (b). In principle, both cases are captured by the model in Eq. (1).

In this formalism (for details, see **Appendix D**), the current-flowing superconducting state can be captured by the finite-momentum pairing order parameter matrix $\hat{\Delta}(\mathbf{k}, \mathbf{q})$ with a center-of-mass momentum \mathbf{q} . For the spin-singlet s-wave pairing, $\hat{\Delta}(\mathbf{k}, \mathbf{q}) = \Delta(\mathbf{q})i\sigma_y$ and for the nematic spin-triplet p-wave pairing, $\hat{\Delta}(\mathbf{k}, \mathbf{q}) = \Delta(\mathbf{q})\sin(k_x)\sigma_x$. $\Delta(\mathbf{q})$ can be determined by the self-consistent gap equation

$$\Delta(\mathbf{q}) = -\frac{U}{N_c} \sum_{\mathbf{k}} \langle \hat{c}_{-\mathbf{k}\downarrow} \hat{c}_{\mathbf{k}+\mathbf{q}\uparrow} \rangle u_{\mathbf{k}}, \qquad (15)$$

where $u_{\mathbf{k}} = 1$ for the s-wave pairing and $u_{\mathbf{k}} = \sin k_x$ for the nematic p-wave pairing. Then we can obtain the minimized Helmholtz free energy density $\mathcal{F}_m(\mathbf{q})$ by substituting solved $\hat{\Delta}(\mathbf{k}, \mathbf{q})$ in Eq. (D9) and the supercurrent can be evaluated by $\vec{j}(\mathbf{q}) = 2e\nabla_{\mathbf{q}}\mathcal{F}_m(\mathbf{q})$.

The numerical results are summarized in Fig. 3(c) and (d), where the curves follow a trend similar to those in Fig. 2(a). The SDE can occur as long as $j_{bias} > 0$, and the USC can be realized when $j_{bias} \geq j_{c+}(\theta) = 0.0034et$ in (c) and $j_{c+}(\theta) = 0.0086et$ in (d). Compared with phenomenological analysis, we numerically verified that the

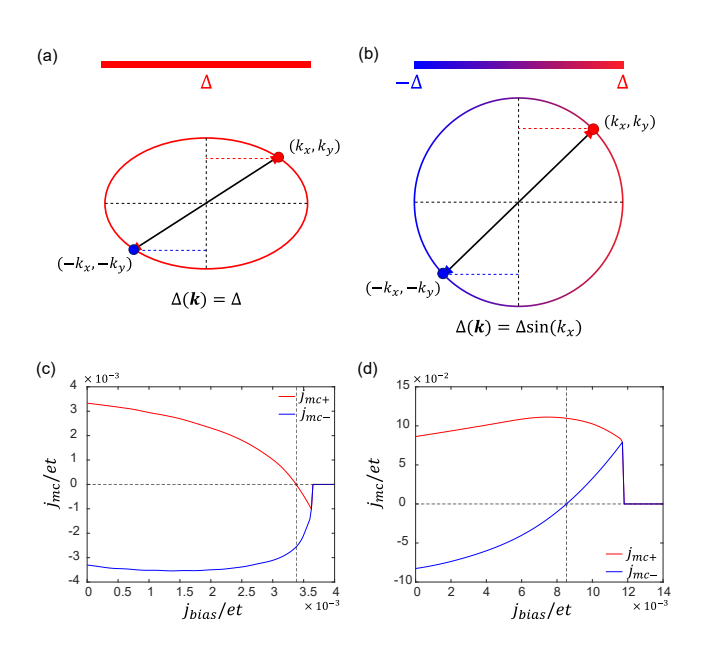


Fig. 3. (a) Schematic illustration of anisotropic Fermi surface with s-wave pairing. (b) Schematic illustration of an isotropic Fermi surface with nematic p-wave pairing. (c) Similar to Fig. 2(a), the results of the square lattice model $(t_x \neq t_y)$ with s-wave pairing, j_{mc+} becomes negative when $j_{bias} > j_{bias,c1} = 0.0034et$. Parameter used here: $\theta = \pi/4, t_x = 0.5t_y = t, \ \mu = 2.5t, \ U = 1.5t$. (d) The results of the square lattice model $(t_x = t_y)$ with p-wave pairing, j_{mc-} becomes positive when $j_{bias} > j_{bias,c1} = 0.0086et$. Parameter used here: $\theta = \pi/4, t_x = t_y = t, \ \mu = 2.5t, \ U = 3.25t$.

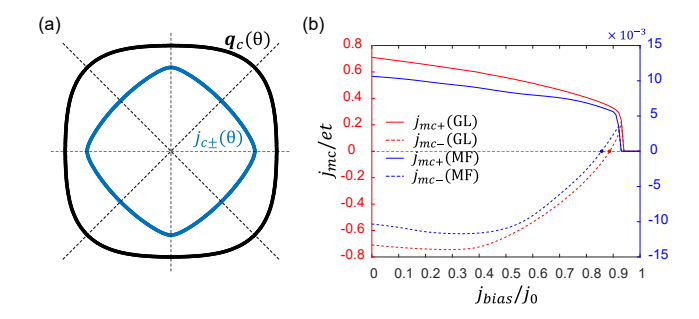


Fig. 4. (a) The black curve shows the envelope of the critical momenta $q_c(\theta)$. The blue curve shows the envelope of the critical current $j_{c\pm}(\theta)$. Both are derived from the GL analysis of the $d_{x^2-y^2}$ -wave superconductor. (b) The evolution of j_{mc+} (solid lines) and j_{mc-} (dashed lines) from the GL analysis (in red) and MF calculations (in blue), j_{bias} is rescaled to [0,1] in arbitrary units j_0 . Parameter used in GL analysis: $\theta=\pi/8, \alpha_0=-t, \beta_0=2t, K_1^d=0.5t, K_2^d=4t, K_3^d=t,$ then $j_{bias,c1}=j_{c+}(\theta)=0.7096et, j_{bias,c1}/j_0=0.8870$ with $j_0=0.8et$, and $Q_{USC}=0.054$. Parameter used in MF calculation: $\theta=\pi/8, t_x=t_y=t, \mu=2.5t, U=3t,$ then $j_{bias,c1}=j_{c+}(\theta)=0.0112et, j_{bias,c1}/j_0=0.8615$ with $j_0=0.013et$ and $Q_{USC}=0.076$.

anisotropies of both the Fermi velocity and the pairing symmetry can lead to DC bias-controlled SDE and USC. A more quantitative verification can be done by comparing Eq. (13) (we denote as $Q_{USC,a}$) with the $Q_{USC,n}$ from direct numerical evaluation. As mentioned before, the m_x/m_y in Eq. (13) can be numerically extracted from $m_x/m_y = (j_{c\pm}(\pi/2)/j_{c\pm}(0))^2$. For the s-wave pairing case, the numerical result $Q_{USC,n}$ matches perfectly with the analytical result $Q_{USC,a}$ ($Q_{USC,n} = Q_{USC,a} = 0.931$). For the p-wave pairing case, $Q_{USC,n} = 0.258$ and $Q_{USC,a} = 0.204$, which are basically in agreement.

VI. HIGH- T_c SUPERCONDUCTOR PLATFORM

Up to now, we have focused on superconductors with two-fold anisotropy. Here we generalize our proposal to a high- T_c SC platform with four-fold anisotropy. The primary advantage of superconducting electronic devices based on high- T_c SC stems from their ability to operate at more economically viable temperatures and a sufficiently wide current operating range due to their large critical currents [57].

We consider the $d_{x^2-y^2}$ -wave pairing case, which transforms under the B_{1g} irreducible representation of the tetragonal point group D_{4h} [58, 59]. Standing as a typical pairing symmetry in cuprate superconductors [59–61], the corresponding GL free energy is

$$F = \int d\mathbf{r} \{\alpha_0 |\Psi|^2 + A_1^d \left(|\partial_x \Psi|^2 + |\partial_y \Psi|^2 \right) + A_2^d |(\partial_x^2 + \partial_y^2) \Psi|^2 + A_3^d |(\partial_x^2 - \partial_y^2) \Psi|^2 + \beta_0 |\Psi|^4.$$
(16)

In momentum space, the free energy density is in the form

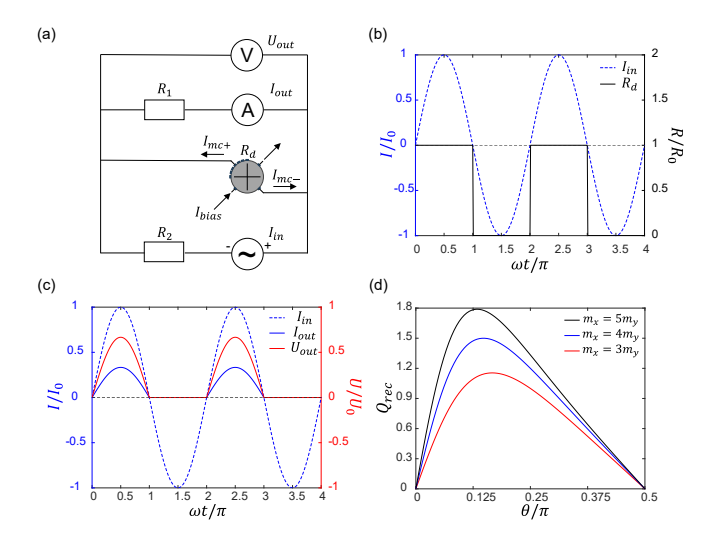


Fig. 5. (a) Circuit schematic of the bias-controlled supercurrent rectifier. The input AC current $I_{in} = I_0 \sin(\omega t)$, the load resistance $R_1 = R_2 = 2R_0$. R_d is the resistance of the CGOST. The rectifier is set to its working regime, so the bias current $j_{bias} = j_{bias,c1}$ and the amplitude of the input current $I_0 \leq j_{mc1}$. (b) The evolution of R_d (black solid line) with the input AC current I_{in} (blue dashed line). (c) The evolution of the output voltage U_{out} (red solid line) and the output current I_{out} (blue solid line) with the input AC current I_{in} (blue dashed line), $U_0 = I_0 R_0$. (d) The quality factor $Q_{rec}(\theta)$ of different effective mass m_x and m_y .

of Eq. (A1) as $\alpha(\mathbf{q}) = \alpha_0 + K_1^d \left(q_x^2 + q_y^2\right) + K_2^d \left(q_x^4 + q_y^4\right) + K_3^d q_x^2 q_y^2$, with the coefficients are redefined as: $K_1^d = A_1^d$, $K_2^d = A_2^d + A_3^d$, $K_3^d = 2A_2^d - 2A_3^d$. The boundary of the physical domain can be determined by Eq. (A5), which is shown in Fig. 4(a) as the black curve, and the envelope of critical currents $j_{c\pm}(\theta)$ is shown in Fig. 4(a) as the blue curve, both have apparent four-fold anisotropy.

Accompanying the GL analysis, we also performed numerical MF calculations with spin-singlet $d_{x^2-y^2}$ -wave pairing, using $u_{\mathbf{k}} = \cos k_x - \cos k_y$ in Eq. (15). Fig. 4(b) shows a comparison between the results of the GL theory (red lines) and the numerical calculations (blue lines), which are in qualitative agreement. This indicates that our phenomenological model and the chosen parameters well capture the essential features of the $d_{x^2-y^2}$ -wave pairing, establishing a foundation for its use in CGOST.

VII. BIAS-CONTROLLED SUPERCURRENT RECTIFIER

Based on previous discussions, we present an example of how to design novel superconducting electronic devices using the CGOST, i.e., a DC bias-controlled superconducting half-wave rectifier.

As schematically shown in Fig. 5(a), in the circuit, the input AC current $I_{in} = I_0 \sin(\omega t)$ is to be rectified, where I_0 is the amplitude and ω is the frequency. Here, to opti-

mize the use of the original current waveform, the applied DC bias should be set to $j_{bias}=j_{bias,c1}$ to ensure an ideal rectification window, and the amplitude of the input current satisfies $I_0 \leq j_{mc1}$. We denote R_d as the resistance of the CGOST, and Fig. 5(b) shows how it evolves under the input current I_{in} . When $I_{in} \leq 0$ the CGOST is in the superconducting regime ($R_d=0$), and when $I_{in}>0$ it is in the normal state ($R_d\approx R_0$). Fig. 5(c) shows the output voltage V_{out} and the output current I_{out} accounting for rectification. Clearly, the circuit we designed works as an optimal superconducting half-wave rectifier.

We define $Q_{rec} = j_{mc1}/j_{bias,c1}$ to measure the quality of the rectifier made from CGOST. A larger Q_{rec} implies a wider rectification window with respect to the activation bias current. In terms of Eq. (2), we can show that (see the details in **SI II** [56]):

$$Q_{rec}(\theta) = \frac{2|m_x - m_y|}{m_x \tan \theta + m_y \cot \theta},$$
 (17)

which provides a simple angle-dependent design rule for the device optimization. The maximum of $Q_{rec}(\theta)$ is located at $\tan \theta = \sqrt{m_y/m_x}$, and $\max(Q_{rec}) = \frac{|m_x - m_y|}{\sqrt{m_y m_x}}$, implying that larger anisotropy gives rise to better rectifier, as shown in Fig. 5(d).

VIII. CONCLUSION AND DISCUSSION

In summary, we have demonstrated that a DC bias can generally induce a tunable transverse SDE and USC in anisotropic superconductors. Our proposal harnesses intrinsic material properties and the underdeveloped multiterminal design [35] to achieve tunable nonreciprocal superconducting transport without explicit symmetry breaking. We expect that our design protocol significantly improves the accessibility of nonreciprocal phenomena in superconducting systems, and also provides a new paradigm for designing novel superconducting devices.

Throughout this work, we assume the j_{bias} is injected from control terminals. However, we note that it can also be created from the Meissner effect as screening currents [62], without extra terminals. This observation suggests different designs for CGOST, leaving room for future exploration.

ACKNOWLEDGEMENTS

The authors thank Ying-Ming Xie, Wen-Yu He, James Jun He, K. T. Law, Akito Daido and Su-Yang Xu for inspiring discussions. This work is supported by the School of Science, the Hong Kong University of Science and Technology.

Appendix A: GL analysis of the generic anisotropic superconductor carrying supercurrent

We start from a generic single-q free energy density written as:

$$\mathcal{F} = \alpha(\mathbf{q})|\Psi_{\mathbf{q}}|^2 + \beta|\Psi_{\mathbf{q}}|^4, \tag{A1}$$

where $\beta > 0$ and $\alpha(q) < 0$ denote the superconducting regime. For simplicity, we neglect the q-dependence in the coefficient of the quartic term.

To calculate the current density, $|\Psi_{\boldsymbol{q}}|^2$ can be determined by minimizing the free energy density: $\frac{\partial \mathcal{F}}{\partial |\Psi_{\boldsymbol{q}}|^2} = 0$, so $|\Psi_{\boldsymbol{q}}|^2 = -\frac{\alpha(\boldsymbol{q})}{2\beta}$ and the minimized free energy density is $\mathcal{F}_m = -\frac{\alpha^2(\boldsymbol{q})}{4\beta}$, then the current density is given by:

$$j(\mathbf{q}) = 2e\nabla_{\mathbf{q}}\mathcal{F}_{m} = -\frac{e\alpha(\mathbf{q})}{\beta} \left(\alpha'_{x}\hat{x} + \alpha'_{y}\hat{y}\right), \quad (A2)$$

where $\alpha_i' = \partial \alpha(\mathbf{q})/\partial q_i$.

Then we consider the critical current along the $\hat{\theta} = (\cos \theta, \sin \theta)$ direction $j_{c\pm}(\theta)$, which is equivalent to find the extreme values of |j(q)| along $\hat{\theta}$, in this case, the components of j(q) satisfy:

$$\frac{j_y(\mathbf{q})}{j_x(\mathbf{q})} = \frac{\alpha_x'}{\alpha_y'} = \tan \theta. \tag{A3}$$

To find the extreme values of |j(q)| with such a constraint, we can use the method of Lagrange multipliers, i.e., $\mathcal{L} = |j(q)| + \lambda(\alpha_x' - \alpha_y' \tan \theta)$. The extreme values can be found by solving the following equations simultaneously:

$$\begin{cases} \alpha_x' = \alpha_y' \tan \theta \\ \frac{\partial \mathcal{L}}{\partial q_x} = \frac{\partial \mathcal{L}}{\partial q_y} = 0 \end{cases}, \tag{A4}$$

so that we can show all the local maxima $q_c(\theta)$ of |j(q)| are located at the curve:

$$2\alpha_x'\alpha_y'\alpha_{xy}'' = (\alpha_x')^2 \alpha_{yy}'' + (\alpha_y')^2 \alpha_{xx}'' + \alpha(\boldsymbol{q}) (\alpha_{xx}''\alpha_{yy}'' - (\alpha_{xy}'')^2),$$
(A5)

where $\alpha_{ij}^{"} = \partial^2 \alpha(\mathbf{q})/\partial q_i \partial q_j$. Then we can set the boundary of the domain for momentum $\mathbf{q} \in \mathcal{D}$ according to Eq. (A5), to contain all physical points, and the critical current can be evaluated with the solutions of Eq. (A4) by $j_{c\pm}(\theta) = \pm |\mathbf{j}(\mathbf{q}_c(\theta))|$.

Then we assume that the bias current is applied along the $\hat{\theta}$ direction, then the radical component j_{\parallel} is:

$$j_{\parallel} = 2e \left(\cos\theta \hat{x} + \sin\theta \hat{y}\right) \cdot \nabla_{\mathbf{q}} \mathcal{F}_{m}$$
$$= -\frac{e\alpha(\mathbf{q})}{\beta} \left(\alpha'_{x} \cos\theta + \alpha'_{y} \sin\theta\right), \tag{A6}$$

and the transverse component j_m is:

$$j_{m} = 2e \left(\sin \theta \hat{x} - \cos \theta \hat{y} \right) \cdot \nabla_{\mathbf{q}} \mathcal{F}_{m}$$
$$= -\frac{e\alpha(\mathbf{q})}{\beta} \left(\alpha'_{x} \sin \theta - \alpha'_{y} \cos \theta \right). \tag{A7}$$

Appendix B: Transverse critical currents at small bias limit

To find the measured critical currents in the transverse direction $j_{mc\pm}$, we can solve Eq. (A5) and Eq. (A6) with $j_{\parallel}=j_{bias}$ simultaneously, to determine the corresponding q_c points. Then, substituting the solutions into Eq. (A7) to get $j_{mc\pm}$. In the context of Eq. (2) of the **Main Text**, Eq. (A5) and Eq. (A6) become $q_x^2/m_x+q_y^2/m_y<2|\alpha|/3$ and Eq. (6).

In the small bias current limit (the higher order terms of j_{bias} are omitted), we can get:

$$\begin{cases}
q_{yc} \approx \pm \sqrt{\frac{2|\alpha|m_y^2}{3\left(m_x \tan^2 \theta + m_y\right)}} \\
+ \frac{3\beta m_x m_y \sin \theta j_{bias}}{2e|\alpha|\left(m_x \sin^2 \theta + m_y \cos^2 \theta\right)}, \\
q_{xc} \approx \frac{m_x}{\cos \theta} \left(\frac{3\beta}{2e|\alpha|} j_{bias} - \frac{q_y \sin \theta}{m_y}\right)
\end{cases}$$
(B1)

And by substituting Eq. (B1) into Eq. (7), the transverse current $j_{mc\pm}$ is given by:

$$j_{mc\pm} = \pm \frac{2e|\alpha|}{3\beta\cos\theta} \sqrt{\frac{2|\alpha|}{3\left(m_x \tan^2\theta + m_y\right)}} + \frac{j_{bias}\left(m_y - m_x\right)}{m_x \tan\theta + m_y \cot\theta}.$$
(B2)

Appendix C: GL theory of a nematic *p*-wave superconductor

We start from considering the GL formalism of a spin-triplet p-wave superconductor with tetragonal point group symmetry D_{4h} . The order parameter can be described by a two-component \vec{d} -vector: $\vec{d}(\mathbf{k}) = \eta_x \hat{z} k_x + \eta_y \hat{z} k_y$, in the gap function $\hat{\Delta}(\mathbf{k}) = i \vec{d}(\mathbf{k}) \cdot \vec{\sigma} \sigma_y$. It transforms under the E_u irreducible representation, and the generic GL free energy is given by [54]:

$$F = \int d\mathbf{r} \{a|\vec{\eta}|^2 + b_1|\vec{\eta}|^4 + \frac{b_2}{2} \{\eta_x^{*2}\eta_y^2 + \eta_x^2\eta_y^{*2}\}$$

$$+ b_3|\eta_x|^2|\eta_y|^2 + K_1 \{|\partial_x\eta_x|^2 + |\partial_y\eta_y|^2\}$$

$$+ K_2 \{|\partial_x\eta_y|^2 + |\partial_y\eta_x|^2\} + K_3 \{(\partial_x\eta_x)^* (\partial_y\eta_y) + c.c.\}$$

$$+ K_4 \{(\partial_x\eta_y)^* (\partial_y\eta_x) + c.c.\} \}.$$
(C1)

If we choose the GL parameters to be $b_3 > |b_2|$ [54], the ground state is a nematic *p*-wave superconductor with the order parameter $\vec{\eta} = (\eta_x, \eta_y) = (\eta, 0)$, which breaks rotation symmetry reducing D_{4h} (tetragonal) to D_{2h} (orthorhombic). And the GL free energy density becomes

$$F = \int d\mathbf{r} \{ a|\eta|^2 + b_1|\eta|^4 + K_1|\partial_x \eta|^2 + K_2|\partial_y \eta|^2 \}, \text{ (C2)}$$

which has exactly the same form as Eq. (1). However, the anisotropic effective masses here $K_1 \neq K_2$ are not inherited from the anisotropic Fermi velocity in the normal state, but originate from the anisotropic form factor of the nematic p-wave pairing.

Appendix D: Formalism of self-consistent MF theory

In this section, we introduce the self-consistent mean-field (MF) theory used in the **Main Text**. The total Hamiltonian is:

$$\hat{H} = \hat{H}_0 + \hat{H}_{\text{int}},\tag{D1}$$

where $\hat{H}_0 = \sum_{\boldsymbol{k}\sigma} \xi_n(\boldsymbol{k}) c_{\boldsymbol{k}\sigma}^{\dagger} c_{\boldsymbol{k}\sigma}$ and

$$\hat{H}_{\text{int}} = -\sum_{\mathbf{k}\mathbf{k}'\mathbf{q}'\sigma\sigma'} U_{\sigma\sigma'}(\mathbf{k}, \mathbf{k}', \mathbf{q}') \hat{c}_{\mathbf{k}+\mathbf{q}'\sigma}^{\dagger} \hat{c}_{-\mathbf{k}\sigma'}^{\dagger} \hat{c}_{-\mathbf{k}'\sigma'} \hat{c}_{\mathbf{k}'+\mathbf{q}'\sigma}.$$
(D2)

The attractive interaction is [6]:

$$U_{\sigma\sigma'}(\mathbf{k}, \mathbf{k}', \mathbf{q}') = U_{\sigma\sigma'}\delta_{\mathbf{q}\mathbf{q}'}u_{\sigma\sigma'}(\mathbf{k})u_{\sigma\sigma'}^*(\mathbf{k}'), \qquad (D3)$$

where q is a finite center-of-mass momentum and $u_{\sigma\sigma'}$ is the form factor.

To describe the current-flowing state, the superconducting order parameter $\Delta_{\sigma\sigma'}(q)$ is considered with a center-of-mass momentum $q = q_x \hat{x} + q_y \hat{y}$. The mean-field decoupling of the attractive interaction yields the following interaction Hamiltonian:

$$\hat{H}_{\text{int}} = \sum_{\mathbf{k}\sigma\sigma'} \Delta_{\sigma\sigma'}(\mathbf{q}) u_{\sigma\sigma'}(\mathbf{k}) c_{\mathbf{k}+\mathbf{q}\sigma}^{\dagger} c_{-\mathbf{k}\sigma'}^{\dagger}$$

$$+ h.c. + \sum_{\mathbf{r}\sigma'} \frac{N_c |\Delta_{\sigma\sigma'}(\mathbf{q})|^2}{U_{\sigma\sigma'}}.$$
(D4)

The full mean-field Hamiltonian can be rewritten in the Nambu basis $\psi(\boldsymbol{k},\boldsymbol{q}) = \left(\hat{c}_{\boldsymbol{k}+\boldsymbol{q}\uparrow},\hat{c}_{\boldsymbol{k}+\boldsymbol{q}\downarrow},\hat{c}_{-\boldsymbol{k}\uparrow}^{\dagger},\hat{c}_{-\boldsymbol{k}\downarrow}^{\dagger}\right)^T$ as

$$\hat{\mathcal{H}}_{\mathrm{MF}} = \sum_{\mathbf{k}} \psi^{\dagger}(\mathbf{k}, \mathbf{q}) \hat{H}_{\mathrm{BdG}}(\mathbf{k}, \mathbf{q}) \psi(\mathbf{k}, \mathbf{q}) + \sum_{\mathbf{k}} \mathrm{Tr}[\hat{H}_{n}(-\mathbf{k})] + \sum_{\mathbf{k}, \mathbf{q}} \frac{N_{c} |\Delta_{\sigma\sigma'}(\mathbf{q})|^{2}}{U_{\sigma\sigma'}}, \tag{D5}$$

where the Bogoliubov–de Gennes (BdG) Hamiltonian $\hat{H}_{\mathrm{BdG}}(k,q)$ reads:

$$\hat{H}_{BdG}(\boldsymbol{k}, \boldsymbol{q}) = \begin{pmatrix} \hat{H}_n(\boldsymbol{k} + \boldsymbol{q}) & \hat{\Delta}(\boldsymbol{k}, \boldsymbol{q}) \\ \hat{\Delta}^{\dagger}(\boldsymbol{k}, \boldsymbol{q}) & -\hat{H}_n(-\boldsymbol{k}) \end{pmatrix}, \quad (D6)$$

with $\hat{H}_n(\mathbf{k}) = \xi_n(\mathbf{k})\mathbf{I}_2$ and the order parameter matrix is defined as:

$$\hat{\Delta}(\boldsymbol{k}, \boldsymbol{q}) = \begin{pmatrix} \Delta_{\uparrow\uparrow}(\boldsymbol{q}) u_{\uparrow\uparrow}(\boldsymbol{k}) & \Delta_{\uparrow\downarrow}(\boldsymbol{q}) u_{\uparrow\downarrow}(\boldsymbol{k}) \\ -\Delta_{\uparrow\downarrow}(\boldsymbol{q}) u_{\uparrow\downarrow}(\boldsymbol{k}) & \Delta_{\downarrow\downarrow}(\boldsymbol{q}) u_{\downarrow\downarrow}(\boldsymbol{k}) \end{pmatrix}. \quad (D7)$$

And the grand potential can be defined as:

$$\Omega[\mu(\boldsymbol{q}), \Delta(\boldsymbol{q}), \boldsymbol{q}] = -\frac{1}{\beta} \log \mathcal{Z} = -\frac{1}{\beta} \ln \text{Tr}[e^{-\beta \hat{\mathcal{H}}_{\text{MF}}}],$$
(D8)

In the canonical ensemble, we transfer to the Helmholtz free energy density \mathcal{F} , which is written as:

$$\mathcal{F}(\boldsymbol{q}) = \frac{1}{N_c} \left(\Omega[\mu(\boldsymbol{q}), \Delta(\boldsymbol{q}), \boldsymbol{q}] + \mu(\boldsymbol{q}) N_c \right)$$
$$= \frac{1}{\beta N_c} \sum_{\boldsymbol{q}, \boldsymbol{k}} \ln \left(1 + e^{-\beta E_n(\boldsymbol{k}, \boldsymbol{q})} \right) + \sum_{\boldsymbol{q}, \boldsymbol{\ell}} \frac{|\Delta_{\sigma \sigma'}(\boldsymbol{q})|^2}{U_{\sigma \sigma'}}.$$
(D9)

where $E_n(\mathbf{k}, \mathbf{q})$ is the n-th eigenvalue of the BdG Hamiltonian $\hat{H}_{\mathrm{BdG}}(\mathbf{k}, \mathbf{q})$. For a given \mathbf{q} , $\Delta(\mathbf{q})$ can be determined self-consistently by solving the gap equation:

$$\Delta_{\sigma\sigma'}(\boldsymbol{q}) = -\frac{U_{\sigma\sigma'}}{N_c} \sum_{\boldsymbol{k}} u_{\sigma\sigma'}^*(\boldsymbol{k}) \left\langle \hat{c}_{-\boldsymbol{k}\sigma'} \hat{c}_{\boldsymbol{k}+\boldsymbol{q}\sigma} \right\rangle. \quad (D10)$$

Then we can obtain the minimized Helmholtz free energy density $\mathcal{F}_m(q)$ by substituting solved $\hat{\Delta}(k,q)$ in Eq. (D9) and the supercurrent can be evaluated by $\vec{j}(q) = 2e\nabla_q \mathcal{F}_m(q)$.

In the main text, we only consider the interaction between electrons with opposite spins, so the explicit forms of $U_{\sigma\sigma'}(\mathbf{k}, \mathbf{k}', \mathbf{q}')$ can be simplified as follows:

$$U_{\sigma\sigma'}(\mathbf{k}, \mathbf{k}', \mathbf{q}') = U(1 - \delta_{\sigma\sigma'})\delta_{\mathbf{q}\mathbf{q}'}u(\mathbf{k})u^*(\mathbf{k}'), \quad (D11)$$

where

$$u(\mathbf{k}) = \begin{cases} 1 & (s\text{-wave}) \\ \sin k_x & (p\text{-wave}) \\ \cos k_x - \cos k_y & (d\text{-wave}) \end{cases}$$
(D12)

The BdG Hamiltonian can be reduced to a 2 by 2 matrix as:

$$\hat{H}_{BdG}(\mathbf{k}, \mathbf{q}) = \begin{pmatrix} \xi_n(\mathbf{k} + \mathbf{q}) & \Delta(\mathbf{q})u(\mathbf{k}) \\ \Delta^*(\mathbf{q})u^*(\mathbf{k}) & -\xi_n(-\mathbf{k}) \end{pmatrix}, \quad (D13)$$

and the gap equation reads:

$$\Delta(\boldsymbol{q}) = -\frac{U}{N_c} \sum_{\boldsymbol{k}} u^*(\boldsymbol{k}) \left\langle \hat{c}_{-\boldsymbol{k}\downarrow} \hat{c}_{\boldsymbol{k}+\boldsymbol{q}\uparrow} \right\rangle. \tag{D14}$$

- [1] F. Ando, Y. Miyasaka, T. Li, J. Ishizuka, T. Arakawa, Y. Shiota, T. Moriyama, Y. Yanase, and T. Ono, Nature 584, 373 (2020).
- [2] Y.-Y. Lyu, J. Jiang, Y.-L. Wang, Z.-L. Xiao, S. Dong, Q.-H. Chen, M. V. Milošević, H. Wang, R. Divan, J. E. Pearson, et al., Nature communications 12, 2703 (2021).
- [3] N. F. Yuan and L. Fu, Proceedings of the National Academy of Sciences 119, e2119548119 (2022).
- [4] J. J. He, Y. Tanaka, and N. Nagaosa, New Journal of Physics 24, 053014 (2022).
- [5] A. Daido, Y. Ikeda, and Y. Yanase, Physical Review Letters 128, 037001 (2022).
- [6] A. Daido and Y. Yanase, Physical Review B 106, 205206 (2022).
- [7] H. Narita, J. Ishizuka, R. Kawarazaki, D. Kan, Y. Shiota, T. Moriyama, Y. Shimakawa, A. V. Ognev, A. S. Samardak, Y. Yanase, et al., Nature Nanotechnology 17, 823 (2022).
- [8] M. Nadeem, M. S. Fuhrer, and X. Wang, Nature Reviews Physics 5, 558 (2023).
- [9] Y. Hou, F. Nichele, H. Chi, A. Lodesani, Y. Wu, M. F. Ritter, D. Z. Haxell, M. Davydova, S. Ilić, O. Glezakou-Elbert, et al., Physical Review Letters 131, 027001 (2023).
- [10] J. J. He, Y. Tanaka, and N. Nagaosa, Nature Communications 14, 3330 (2023).
- [11] K. Nakamura, A. Daido, and Y. Yanase, Physical Review B 109, 094501 (2024).
- [12] A. Daido and Y. Yanase, Physical Review B 111, L020508 (2025).
- [13] J.-X. Hu, S. A. Chen, and K. Law, Physical Review B 111, 174513 (2025).
- [14] U. Nagata, M. Aoki, A. Daido, S. Kasahara, Y. Kasahara, R. Ohshima, Y. Ando, Y. Yanase, Y. Matsuda, and M. Shiraishi, Physical Review Letters 134, 236703 (2025).
- [15] Y. Asano, Y. Tanaka, M. Sigrist, and S. Kashiwaya, Physical Review B 67, 184505 (2003).
- [16] C.-Z. Chen, J. J. He, M. N. Ali, G.-H. Lee, K. C. Fong, and K. Law, Physical Review B 98, 075430 (2018).
- [17] K. Misaki and N. Nagaosa, Physical Review B 103, 245302 (2021).
- [18] J. Van Ostaay, A. Akhmerov, and C. Beenakker, Physical Review B 83, 195441 (2011).
- [19] Y.-B. Choi, Y. Xie, C.-Z. Chen, J. Park, S.-B. Song, J. Yoon, B. J. Kim, T. Taniguchi, K. Watanabe, J. Kim, et al., Nature Materials 19, 974 (2020).
- [20] Y. Tanaka, B. Lu, and N. Nagaosa, Physical Review B 106, 214524 (2022).
- [21] K.-R. Jeon, J.-K. Kim, J. Yoon, J.-C. Jeon, H. Han, A. Cottet, T. Kontos, and S. S. Parkin, Nature Materials 21, 1008 (2022).
- [22] B. Pal, A. Chakraborty, P. K. Sivakumar, M. Davydova, A. K. Gopi, A. K. Pandeya, J. A. Krieger, Y. Zhang, M. Date, S. Ju, et al., Nature physics 18, 1228 (2022).
- [23] L. Bauriedl, C. Bäuml, L. Fuchs, C. Baumgartner, N. Paulik, J. M. Bauer, K.-Q. Lin, J. M. Lupton, T. Taniguchi, K. Watanabe, et al., Nature communications 13, 4266 (2022).
- [24] C. Baumgartner, L. Fuchs, A. Costa, S. Reinhardt, S. Gronin, G. C. Gardner, T. Lindemann, M. J. Manfra,

- P. E. Faria Junior, D. Kochan, et al., Nature nanotechnology 17, 39 (2022).
- [25] M. Davydova, S. Prembabu, and L. Fu, Science advances 8, eabo0309 (2022).
- [26] Y. Zhang, Y. Gu, P. Li, J. Hu, and K. Jiang, Physical Review X 12, 041013 (2022).
- [27] J. Díez-Mérida, A. Díez-Carlón, S. Yang, Y.-M. Xie, X.-J. Gao, J. Senior, K. Watanabe, T. Taniguchi, X. Lu, A. P. Higginbotham, et al., Nature Communications 14, 2396 (2023).
- [28] Y.-M. Xie, D. K. Efetov, and K. T. Law, Physical Review Research 5, 023029 (2023).
- [29] J.-X. Hu, Z.-T. Sun, Y.-M. Xie, and K. T. Law, Physical Review Letters 130, 266003 (2023).
- [30] M. Gupta, G. V. Graziano, M. Pendharkar, J. T. Dong, C. P. Dempsey, C. Palmstrøm, and V. S. Pribiag, Nature communications 14, 3078 (2023).
- [31] M. Trahms, L. Melischek, J. F. Steiner, B. Mahendru, I. Tamir, N. Bogdanoff, O. Peters, G. Reecht, C. B. Winkelmann, F. von Oppen, et al., Nature 615, 628 (2023).
- [32] B. Lu, S. Ikegaya, P. Burset, Y. Tanaka, and N. Nagaosa, Physical Review Letters 131, 096001 (2023).
- [33] S. Ilić, P. Virtanen, D. Crawford, T. T. Heikkilä, and F. S. Bergeret, Physical Review B 110, L140501 (2024).
- [34] J. Cayao, N. Nagaosa, and Y. Tanaka, Physical Review B 109, L081405 (2024).
- [35] W. Zeng, Physical Review Letters 134, 176002 (2025).
- [36] A. Daido and Y. Yanase, Physical Review Research 6, L022009 (2024).
- [37] M. Castellani, O. Medeiros, A. Buzzi, R. A. Foster, M. Colangelo, and K. K. Berggren, Nature Electronics, 1 (2025).
- [38] J. Ingla-Aynés, Y. Hou, S. Wang, E.-D. Chu, O. A. Mukhanov, P. Wei, and J. S. Moodera, Nature Electronics, 1 (2025).
- [39] C. Sun and A. Bezryadin, arXiv preprint arXiv:2507.09478 (2025).
- [40] J. Lu, O. Zheliuk, I. Leermakers, N. F. Yuan, U. Zeitler, K. T. Law, and J. Ye, Science 350, 1353 (2015).
- [41] Y. Saito, Y. Nakamura, M. S. Bahramy, Y. Kohama, J. Ye, Y. Kasahara, Y. Nakagawa, M. Onga, M. Tokunaga, T. Nojima, et al., Nature Physics 12, 144 (2016).
- [42] X. Xi, Z. Wang, W. Zhao, J.-H. Park, K. T. Law, H. Berger, L. Forró, J. Shan, and K. F. Mak, Nature Physics 12, 139 (2016).
- [43] B. T. Zhou, N. F. Yuan, H.-L. Jiang, and K. T. Law, Physical Review B 93, 180501 (2016).
- [44] W.-Y. He, B. T. Zhou, J. J. He, N. F. Yuan, T. Zhang, and K. T. Law, Communications Physics 1, 40 (2018).
- [45] D. A. Rhodes, A. Jindal, N. F. Yuan, Y. Jung, A. Antony, H. Wang, B. Kim, Y.-c. Chiu, T. Taniguchi, K. Watanabe, et al., Nano letters 21, 2505 (2021).
- [46] X.-Z. Li, Z.-B. Qi, Q. Wu, and W.-Y. He, Communications Physics 7, 396 (2024).
- [47] H. Zhao, H. Li, B. R. Ortiz, S. M. Teicher, T. Park, M. Ye, Z. Wang, L. Balents, S. D. Wilson, and I. Zeljkovic, Nature 599, 216 (2021).
- [48] X. Feng, K. Jiang, Z. Wang, and J. Hu, Science bulletin 66, 1384 (2021).
- [49] T. Neupert, M. M. Denner, J.-X. Yin, R. Thomale, and

- M. Z. Hasan, Nature Physics 18, 137 (2022).
- [50] L. Nie, K. Sun, W. Ma, D. Song, L. Zheng, Z. Liang, P. Wu, F. Yu, J. Li, M. Shan, et al., Nature 604, 59 (2022).
- [51] J.-X. Yin, B. Lian, and M. Z. Hasan, Nature 612, 647 (2022).
- [52] R. Soto-Garrido and E. Fradkin, Physical Review B 89, 165126 (2014).
- [53] V. Kozii, H. Isobe, J. W. Venderbos, and L. Fu, Physical Review B 99, 144507 (2019).
- [54] M. Sigrist and K. Ueda, Reviews of Modern physics 63, 239 (1991).
- [55] L. Šmejkal, R. González-Hernández, T. Jungwirth, and J. Sinova, Science advances 6, eaaz8809 (2020).
- [56] The Supplementary Information for "Current-Gated Orthogonal Superconducting Transistor", which includes two parts: I. Requirements for the DC bias induced USC; II. Derivation of the unidirectional superconductivity quality factor Q_{USC} and rectification quality factor Q_{rec} .
- [57] J. Orenstein and A. Millis, Science 288, 468 (2000).
- [58] Q.-G. Yang, D. Wang, and Q.-H. Wang, Physical Review B 108, L140505 (2023).
- [59] H. Won and K. Maki, Physical Review B 49, 1397 (1994).
- [60] C. Tsuei and J. Kirtley, Reviews of Modern Physics 72, 969 (2000).
- [61] A. Damascelli, Z. Hussain, and Z.-X. Shen, Reviews of modern physics 75, 473 (2003).
- [62] M. Tinkham, Introduction to superconductivity (Courier Corporation, 2004).

Supplementary Information for "Current-Gated Orthogonal Superconducting Transistor"

Ruo-Peng Yu, ¹ Jin-Xin Hu, ¹ Zi-Ting Sun ¹

¹Department of Physics, The Hong Kong University of Science and Technology, Clear Water Bay, Hong Kong, China

I. REQUIREMENTS FOR THE DC BIAS INDUCED USC

In this section, we consider the condition for USC. When the bias is injected in the direction $\hat{\theta} = (\cos \theta, \sin \theta)$, we note that $j_m \leq 0$ is equivalent to

$$\alpha_x' \sin \theta \le \alpha_y' \cos \theta. \tag{S1}$$

Let l be the curve determined by the equation: $j_{\parallel}(q_x,q_y)=j_{bias}$. If all points $(q_x,q_y)\in l$ satisfy Eq. (S1) and $l\in\mathcal{D}$, where \mathcal{D} is the physical domain of (q_x,q_y) , then the USC along the transverse direction can be achieved. In the context of **Main Text**, we have mentioned that \mathcal{D} is:

$$\frac{q_x^2}{m_x} + \frac{q_y^2}{m_y} \le \frac{2|\alpha|}{3},\tag{S2}$$

If $j_m \leq 0$, then $\frac{q_x \sin \theta}{m_x} \leq \frac{q_y \cos \theta}{m_y}$, so we have:

$$q_y \ge \left(\frac{m_y}{m_x} \tan \theta\right) q_x = k_\theta q_x,$$
 (S3)

where $k_{\theta} = \frac{m_y}{m_x} \tan \theta$. As shown in Fig. S1(a), the line $q_y = k_{\theta}q_x$ (white line) divides the domain into a positive region and a negative region of j_m , within the red area and the blue area, respectively. Let l_i be the curve determined by the equation: $j_{\parallel}(q_x, q_y) = j_{bias,i}$. If all the points on l_i fall into one side of the region, we say the USC in the transverse direction occurs.

Seeking a better understanding of this problem, we show the variation of the curves l_i (i=1,2,3) with increasing $j_{bias,i}$ in Fig. S1(a). The middle curve (l_2) satisfies $j_{bias,2} = j_{c+}(\theta)$, and the white line $q_y = k_\theta q_x$ is the tangent of l_2 . For $j_{bias,1} < j_{c+}(\theta)$, l_1 crosses both the blue and red areas, so j_m can be either negative or positive. But for $j_{bias,3} > j_{c+}(\theta)$, l_3 is fully inside the blue area, which means j_m can only be negative. We then conclude that the minimal bias current needed to establish the USC is $j_{bias,c1} = j_{c+}(\theta)$, and the measured transverse current j_m becomes unidirectional only when $j_{bias} \ge j_{c+}(\theta)$, which is consistent with the discussions in Main Text.

II. DERIVATION OF THE UNIDIRECTIONAL SUPERCONDUCTIVITY QUALITY FACTOR AND RECTIFICATION QUALITY FACTOR

In this section, we want to derive $Q_{USC} = 1 - j_{bias,c1}/j_{bias,c2}$ and $Q_{rec} = j_{mc1}/j_{bias,c1}$. As we already knew that $j_{bias,c1} = j_{c+}(\theta)$, here we only need to derive $j_{bias,c2}$ and j_{mc1} .

To determine $j_{bias,c2}$, we note that the curve $j_{\parallel}(q_x,q_y)=j_{bias,c2}$ and the domain boundary $q_x^2/m_x+q_y^2/m_y=2|\alpha|/3$ share only one intersection point, so if we combine these two equations, we can obtain the quadratic equation:

$$\frac{m_x}{\cos^2 \theta} \left(\frac{3\beta}{2e|\alpha|} j_{bias,c2} - \frac{q_y \sin \theta}{m_y} \right)^2 + \frac{q_y^2}{m_y} = \frac{2|\alpha|}{3}.$$
 (S4)

When this quadratic equation has only one solution, the discriminant must be 0, so we can obtain

$$j_{bias,c2} = \frac{e}{\beta} \left(\frac{2|\alpha|}{3}\right)^{3/2} \sqrt{\frac{\cos^2 \theta}{m_x} + \frac{\sin^2 \theta}{m_y}}.$$
 (S5)

Then q_y is given by:

$$q_y = \sqrt{\frac{2|\alpha|}{3}} \sqrt{\frac{m_x m_y \sin^2 \theta}{m_x \sin^2 \theta + m_y \cos^2 \theta}},$$
 (S6)

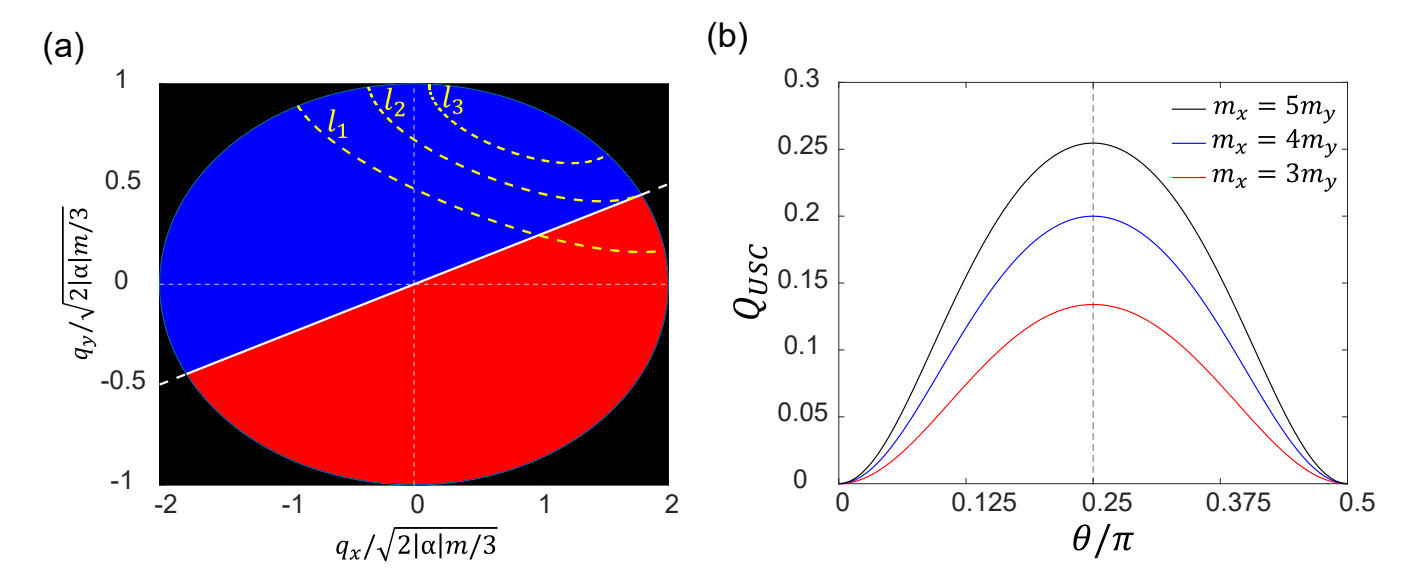


Fig. S1. (a) The distribution of $j_m(q_x, q_y)$ (the black area is out of the domain), $j_m \leq 0$ inside the blue area, and $j_m \geq 0$ inside the red area. The yellow dotted curves l_i (i=1,2,3) show the curves decided by the equation: $j_{\parallel}(q_x, q_y) = j_{bias}$ with specific j_{bias} ($j_{bias,1} = 0.9et, j_{bias,2} = 1.217et$ and $j_{bias,3} = 1.4et$). (b) The quality factor $Q_{USC}(\theta)$ of different effective mass m_x and m_y , $Q(\theta)$ always has a local maximum at $\theta = \pi/4$. Parameter used here: $\theta = \pi/4, \alpha = -0.5t, \beta = 0.1t, m_x = 4/t, m_y = 1/t$. Then $j_{bias,c1} = j_{c+}(\theta) = 1.217et$.

and we know (q_x, q_y) is located at the boundary: $q_x^2/m_x + q_y^2/m_y = 2|\alpha|/3$, so

$$q_x = \sqrt{\frac{2|\alpha|}{3}} \sqrt{\frac{m_x m_y \cos^2 \theta}{m_x \sin^2 \theta + m_y \cos^2 \theta}}.$$
 (S7)

From $j_m(q_x, q_y)$, j_{mc2} is

$$j_{mc2} = \frac{e}{\beta} \left(\frac{2|\alpha|}{3}\right)^{3/2} \frac{(m_y - m_x)\sin\theta\cos\theta}{\sqrt{(m_x\sin^2\theta + m_y\cos^2\theta)m_xm_y}}.$$
 (S8)

In terms of $j_{bias,c1} = j_{c+}(\theta)$ and $j_{bias,c2}$, we have

$$Q_{USC} = 1 - \sqrt{\frac{m_x m_y}{(m_x \cos^2 \theta + m_y \sin^2 \theta)(m_y \cos^2 \theta + m_x \sin^2 \theta)}}.$$
 (S9)

And Q_{USC} for different (θ, m_x, m_y) is plotted in Fig. S1(b). As we explained in the **Main Text**, Q_{USC} is peaked at $\theta = \pi/4$ and globally increases with the anisotropy.

To get j_{mc1} , we can solve the following equations simultaneously:

$$\begin{cases}
j_{bias,c1} = -\frac{e}{\beta} \left[\alpha + \frac{1}{2} \left(\frac{q_x^2}{m_x} + \frac{q_y^2}{m_y} \right) \right] \left(\frac{q_x \cos \theta}{m_x} + \frac{q_y \sin \theta}{m_y} \right) \\
\frac{q_x^2}{m_x} + \frac{q_y^2}{m_y} = \frac{2|\alpha|}{3}
\end{cases},$$
(S10)

one solution of (q_x, q_y) corresponds to the case $j_m = 0$, and the other solution is

$$\begin{cases}
q_y = \frac{m_x + (m_x - m_y)\cos^2\theta}{m_x\sin^2\theta + m_y\cos^2\theta} \frac{\sqrt{2|\alpha|}m_y\sin\theta}{\sqrt{3(m_x\cos^2\theta + m_y\sin^2\theta)}}, \\
q_x = \frac{m_x}{\cos\theta} \left(\frac{3\beta}{2e|\alpha|}j_{bias,c1} - \frac{q_y\sin\theta}{m_y}\right)
\end{cases} (S11)$$

and then j_{mc1} can be determined as:

$$j_{mc1} = \frac{4e|\alpha||m_x - m_y|}{3\beta} \sqrt{\frac{2|\alpha|}{3(m_x \cos^2 \theta + m_y \sin^2 \theta)}} \frac{\tan \theta}{m_x \tan^2 \theta + m_y},$$
 (S12)

at the same time we can obtain

$$Q_{rec}(\theta) = \frac{j_{mc1}}{j_{bias,c1}} = \frac{2|m_x - m_y| \tan \theta}{m_x \tan^2 \theta + m_y}.$$
 (S13)